2
Stability

The industrial revolution in Europe followed the introduction of prime movers, or self-driven machines. It was marked by the invention of advanced grain mills, furnaces, boilers, and the steam engine. These devices could not be adequately regulated by hand, and so arose a new requirement for automatic control systems. A variety of control devices was invented, including float regulators, temperature regulators, pressure regulators, and speed control devices. In the mid-1800s mathematics was first used to analyze the stability of these feedback control systems. In 1840, G.B. Airy discovered that an improper design of the feedback control loop leads to wild oscillations. He was the first to discuss this instability of the control system by using differential equations [1]. Later, J.C. Maxwell in 1868 analyzed the stability of steam engine regulating devices then known as governors [157]. His technique was to linearize the differential equations of motion to find the characteristic equation of the system. He studied the effect of the system parameters on stability and showed that the system is stable if the roots of the characteristic equation have negative real parts.[1]

[1] Maxwell raised the mathematical question of whether a given polynomial of order n and real coefficients has roots with negative real parts and if we could find a solution that can be expressed solely in terms of the coefficients, thus avoiding the explicit computations of the roots. He was not aware that the problem had already been solved in 1856 by Hermite [91]. In 1877, the applied mathematician E. J. Routh provided a numerical technique for determining when a characteristic equation has stable roots [198]. Unaware of the work of Maxwell and Routh, A. B. Stodola posed the problem of determining the stability of the characteristic equation to A. Hurwitz [104] in 1895. Hurwitz

The principal difficulty in studying DDEs lies in the transcendental character of the characteristic equation leading to an infinite number of complex roots. A delay problem connected to the position control of mechanical devices where the number of roots is finite is analyzed below. But, in general, we need to solve the characteristic equation using numerical methods and graphical tools. Often, we are interested in studying the bifurcation diagram of the pulsating solutions in a finite domain of parameters. Then, most of the difficulties of determining the complete spectrum can be set aside, because only a few eigenvalues will contribute to the observed oscillations. In the next section, we analyze the characteristic equation of a simple linear DDE and identify particular points where a change of stability occurs.

2.1 The characteristic equation

We wish to determine all the solutions of a linear DDE such as Eq.(1.3). Redefining the time variable as $t \to t/\tau$, Eq.(1.3) can be rewritten in a simpler form as

$$\frac{dy}{dt} = ay(t-1), \tag{2.1}$$

where

$$a \equiv k\tau \tag{2.2}$$

is our control parameter. Eq.(2.1) is linear which suggests trying an exponential solution of the form

$$y = c\exp(\sigma t). \tag{2.3}$$

Substituting (2.3) into Eq. (1.3) leads to an equation for the growth rate σ, called the *characteristic equation,* given by

$$\sigma - a\exp(-\sigma) = 0. \tag{2.4}$$

Equation (2.4) is a *transcendental equation* and admits several roots.[2] We separate the case σ real and the case σ complex.

---

gave a solution in terms of determinants on the basis of the Hermite paper. Modern proofs may be found in Uspenky [232].

[2] The solution of this equation is known in terms of the Lambert function $W(x)$ that satisfies the equation $W(x)\exp(W(x)) = x$. The solution of Eq.(2.4) with a real then is $\sigma = W(a)$. In symbolic software packages such as Maple and MATLAB, $W(x)$ is a standard function now.

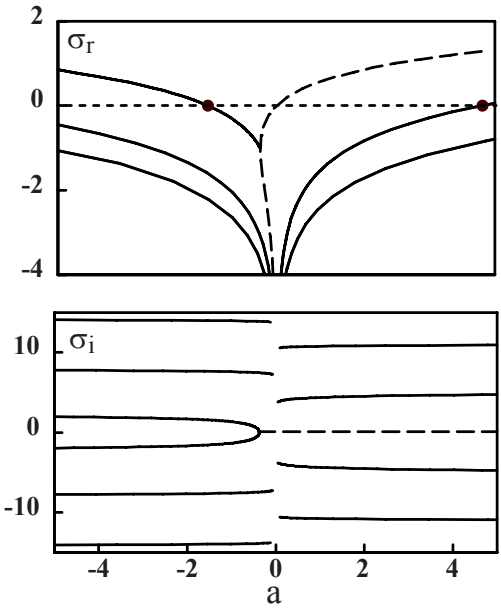

FIGURE 2.1. The solutions of the characteristic equation. The full and broken lines correspond to σ complex and σ real, respectively. Each σ exhibits the limit $\sigma_r \to -\infty$ as $|a| \to 0$. We note that all the σ_r are negative in the interval $-\pi/2 \leq a \leq 0$ meaning stability of the zero solution. The two dots mark the point where one σ_r changes sign.

2.1.1 Roots

1. σ is real. From Eq. (2.4), we have the implicit solution

$$a = \sigma \exp(\sigma). \tag{2.5}$$

Studying the function $a = a(\sigma)$ given by (2.5), we find that σ is a single positive root if $a > 0$ and that there exist two distinct negative roots if $a_c < a < 0$, where $a_c \equiv -e^{-1}$. If $a = a_c$, we have a double root ($\sigma = -1$) and, if $a < a_c$, there exist no real roots. See Figure 2.1.
2. σ is complex. Substituting $\sigma = \sigma_r + i\sigma_i$ into Eq. (2.4) and separating real and imaginary parts, we obtain two equations for σ_r and σ_i given by

$$\sigma_r - a\exp(-\sigma_r)\cos(\sigma_i) = 0, \tag{2.6}$$
$$\sigma_i + a\exp(-\sigma_r)\sin(\sigma_i) = 0. \tag{2.7}$$

Eliminating the common coefficient $a\exp(-\sigma_r)$ leads to the following equation

$$\cot(\sigma_i) = -\frac{\sigma_r}{\sigma_i} \tag{2.8}$$

that contains no parameter. Using (2.8) and then (2.7), the solution can be analyzed in parametric form as (σ_i is the parameter)

$$\sigma_r = -\sigma_i \cot(\sigma_i), \tag{2.9}$$

$$a = -\frac{\sigma_i \exp(\sigma_r)}{\sin(\sigma_i)}. \tag{2.10}$$

See Figure 2.1.

In summary, the solution of Eq. (2.1) can be described as a sum of exponentials of the form

$$y = \sum_n c_n \exp(\sigma_n t) \tag{2.11}$$

where the c_n are unknown. The coefficients c_n can be determined in terms of the initial function $y_0(t)$ $(-1 \leq t < 0)$ using the Laplace transform [21]. Practically, we wish to know if $y \to 0$ as $t \to \infty$ meaning that the determination of the σ_n is good enough ($Re(\sigma_n) < 0$ for all n).

2.1.2 Hopf bifurcation point

At critical values of a, we note that $\sigma_r = 0$ but $\sigma_i \neq 0$. From Eqs. (2.6) and (2.7) with $\sigma_r = 0$, we find the conditions $\cos(\sigma_i) = 0$ and $a = -\sigma_i / \sin(\sigma_i)$ which imply

$$\sigma_i = \pm\pi/2 + k\pi \quad \text{and} \quad a = \mp\sigma_i \tag{2.12}$$

where $k \in Z$. The two first points $a = -\pi/2$ and $a = 3\pi/2$ are indicated in Figure 2.1.

For the logistic equation (1.23), we know that $y = 1$ is a steady-state solution. We may investigate its stability with respect to small perturbations by introducing the deviation

$$u = y - 1 \tag{2.13}$$

into Eq. (1.23). We obtain the following equation for u,

$$\frac{du}{dt} = -\lambda(1 + u)u(t - 1). \tag{2.14}$$

We next assume that $|u|$ is sufficiently small so that $1 + u \simeq 1$. Equation (2.14) then simplifies as

$$\frac{du}{dt} = -\lambda u(t - 1). \tag{2.15}$$

Equation (2.15) is identical to Eq. (2.1) with $y = u$ and $a = -\lambda$. Because the zero solution is stable in the interval $-\pi/2 < a < 0$, we conclude that $y = 1$ is stable if

$$0 < \lambda < \pi/2. \tag{2.16}$$

The critical point $\lambda = \pi/2$ is a Hopf bifurcation point that leads to a branch of periodic solutions (see Chapter 3).

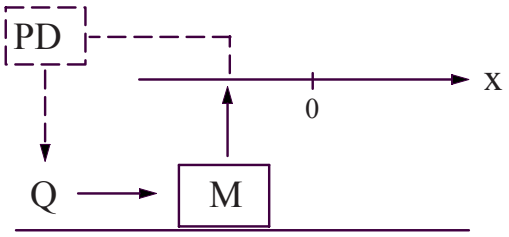

FIGURE 2.2. Position control. The position of mass M is sensed and a control force Q is applied to push the mass into the desired position. The control PD has proportional and differential gains (redrawn from [110]).

2.2 Position control and sampling

Position control is a frequent mechanical controlling problem in robotics. The aim is to drive the robot arm into a desired position. To achieve a clear picture about the behavior of the control, digital effects, such as sampling, should also be included in the mechanical model. Sampling is a kind of delay in information transmission that often leads to unstable oscillations. Analytical investigations of simple models with one degree of freedom play a central role in understanding technical phenomena and designing a safe system. Another example of sampling is described in Chapter 5. Here, we reproduce the analysis by Insperger and Stépán [110] of a simple position control problem. Only the characteristic equation is modified in order to use Hurwitz stability conditions.

Because of the digital sampling effect, the evolution equation is a DDE but the stability problem can be reduced to a finite eigenvalue problem. The system is described by (see Figure 2.2)

$$M\frac{d^2x}{dt'^2} = Q, \tag{2.17}$$

where prime means differentiation with respect to time t'. The sampling time is τ. At each time $t' = n\tau$, the control force Q is quasi-instantaneously readjusted in terms of the observed position $x(t_n)$ and observed velocity $dx(t_n)/dt'$. The control law is

$$Q = -Px(t_n) - D\frac{dx}{dt'}(t_n), \tag{2.18}$$

where P and D are positive coefficients. Introducing the dimensionless time

$$t = t'/\tau, \tag{2.19}$$

Eqs. (2.17) and (2.18) take the simpler form

$$x'' = -px(n) - dx'(n), \tag{2.20}$$

where prime means differentiation with respect to time t. The dimensionless parameters p and d are defined by

$$p = \frac{P\tau^2}{M} \quad \text{and} \quad d = \frac{D\tau}{M}. \tag{2.21}$$

Knowing position $x_n = x(n)$, velocity $v_n = x'(n)$, and acceleration $a_n = x''(n) \equiv -px(n) - dx'(n)$ at time $t = n$, we integrate Eq.(2.20) and obtain

$$\begin{aligned} x'' &= a_n, && (2.22)\\ x' &= v_n + a_n(s-n), && (2.23)\\ x &= x_n + v_n(s-n) + \frac{a_n}{2}(s-n)^2. && (2.24) \end{aligned}$$

Consequently, we determine $x_{n+1} = x(n+1)$, $v_{n+1} = x'(n+1)$, and $a_{n+1} = x''(n+1)$ at time $t = n+1$. The resulting equations form a system of three first-order difference equations of the form

$$\begin{pmatrix} x_{n+1} \\ v_{n+1} \\ a_{n+1} \end{pmatrix} = \begin{pmatrix} 1 & 1 & \frac{1}{2} \\ 0 & 1 & 1 \\ -p & -d & 0 \end{pmatrix} \begin{pmatrix} x_n \\ v_n \\ a_n \end{pmatrix}. \tag{2.25}$$

We wish to analyze the stability of the zero solution. To this end, we seek a solution of the form

$$x_{n+1} = zx_n, \; v_{n+1} = zv_n \quad \text{and} \quad a_{n+1} = za_n, \tag{2.26}$$

where z is called the amplification factor. Substituting (2.26) into (2.25), we obtain the following homogeneous system of equations for x_n, v_n and a_n,

$$\begin{pmatrix} 1-z & 1 & \frac{1}{2} \\ 0 & 1-z & 1 \\ -p & -d & -z \end{pmatrix} \begin{pmatrix} x_n \\ v_n \\ a_n \end{pmatrix} = 0. \tag{2.27}$$

This system of equations has a nontrivial solution if the determinant of the coefficients vanishes. Expanding the determinant as a polynomial in z yields

$$z^3 - 2z^2 + z(1 + \frac{p}{2} + d) + \frac{p}{2} - d = 0. \tag{2.28}$$

This polynomial is known as the amplification polynomial. It is called stable if all the roots lie on or inside the unit circle in the complex z plane:

$$|z_1| \le 1, \quad |z_2| \le 1, \quad |z_3| < 1. \tag{2.29}$$

We next transform Eq.(2.28) to a Hurwitz polynomial to apply a more traditional stability test. A polynomial is called Hurwitz if the location of its roots in the left-hand plane $Re(s) \le 0$ determines stability. To transform Eq.(2.28) to a Hurwitz polynomial, we use the conformal involutory transformation

$$z = \frac{1+s}{1-s}. \tag{2.30}$$

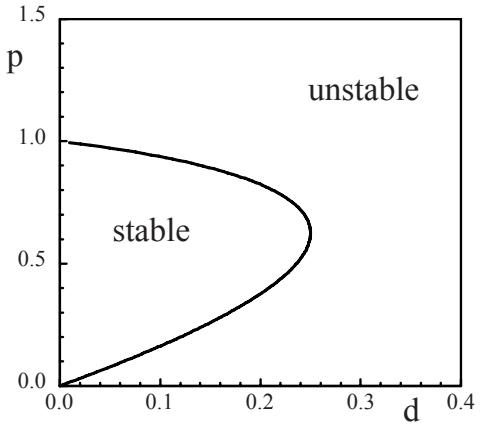

FIGURE 2.3. Position control. The Hopf bifurcation line $p = p_H$ delimits the region of stability.

Inserting (2.30) into (2.28), we obtain

$$s^3(4+2d) + s^2(4+p-4d) + s(-2p+2d) + p = 0. \tag{2.31}$$

The Routh—Hurwitz stability conditions for the third-order polynomial

$$b_3 s^3 + b_2 s^2 + b_1 s + b_0 = 0 \tag{2.32}$$

are given by

$$b_1 > 0, \quad b_1 b_2 - b_0 b_3 > 0 \quad \text{and} \quad b_3 > 0. \tag{2.33}$$

The last condition is always satisfied because $d > 0$. The first condition requires that $d > p$ and the second condition leads to the inequality

$$p^2 + p(6-4d) + 4d(d-1) < 0, \tag{2.34}$$

or equivalently,

$$0 \le p < p_H = -3 + 2d + \sqrt{9-8d}$$

because $p \ge 0$. The critical point $p = p_H$ corresponds to a Hopf bifurcation. This can be verified by substituting $s = i\omega$ ($\omega \neq 0$) into Eq. (2.32) and separating the real and imaginary parts. We find the two conditions $-b_3\omega^2 + b_1 = 0$ and $-b_2\omega^2 + b_0 = 0$, or equivalently,

$$b_1 b_2 - b_0 b_3 = 0 \quad \text{and} \quad \omega^2 = b_1/b_3 > 0. \tag{2.35}$$

The first condition is verified by $p = p_H(d)$ and the second condition provides the square of the Hopf bifurcation frequency

$$\omega^2 = \frac{p_H}{1 - 2d + \sqrt{9-8d}} > 0. \tag{2.36}$$

See Figure 2.3.

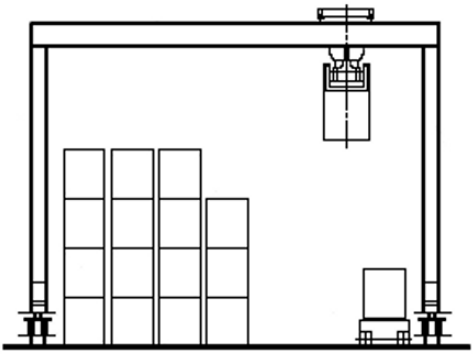

FIGURE 2.4. Rail-mounted gantry cranes are used as yard cranes. Except for the immediate loading or unloading tasks, all operations must be done automatically with an efficient anti-sway control technique (from Erneux and Kalmár-Nagy [60]).

2.3 Reduction of payload oscillations

Gantry cranes are used for moving objects within shipyards, ports, railyards, factories, and warehouses. See Figure 2.4. Gantry cranes can lift several hundred tons and can have spans of well over 50 meters. For fabrication and freight-transfer applications, it is important for the crane to move payloads rapidly and smoothly. If the gantry moves too fast the payload may start to sway, and it is possible for the crane operator to lose control of the payload. During the last four decades, different strategies of controlling payload pendulations without including the operator in the control loop have been investigated. Recently, the question was raised whether a delayed feedback control could be superior to conventional techniques. Henry et al [90] and Masoud et al [154]–[156] developed a control strategy based on a time-delayed position feedback of the payload cable angles. The efficiency of this technique was investigated by both numerical simulations of detailed mathematical models and by experiments in the laboratory [90, 172]. In [60], we have analyzed the possible bifurcations of the crane–payload system subject to a delayed control. We have shown that because of subcritical bifurcations, stable time-periodic attractors may coexist with a stable equilibrium. For safe control of the crane pendulations, such time-periodic regimes should be avoided by using a physical model and finding conditions for safe operation.

In [60], the model was derived using a Lagragian approach. In this section, we consider a simpler model using Newtonian laws. The main forces controlling the crane–payload system are displayed in Figure 2.5. We assume that the cable is inextensible or its length is slowly varying compared to the time-scale of the payload oscillations. The crane is assumed to ride

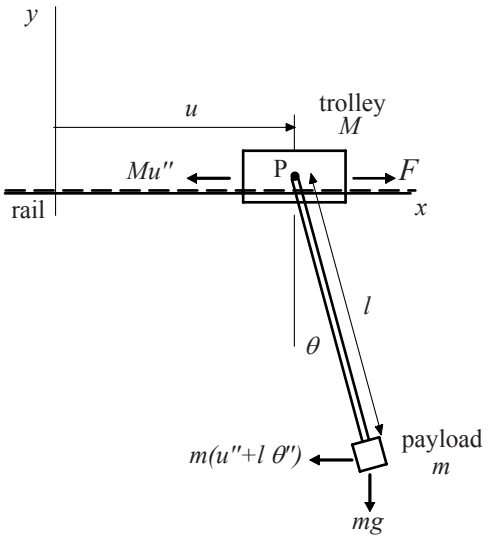

FIGURE 2.5. Simplest pendulum model for a container crane.

on frictionless rails and the payload is assumed to rotate about a frictionless pivot P. The force applied to the motor is $F(t)$. The inertial force on the crane is Mu''. The inertial force on the payload, in the horizontal direction, is $m(u'' + l\theta'')$ and the gravity force on the payload is simply mg. Balancing forces in the horizontal direction ($\Sigma F_x = 0$) gives

$$Mu'' + m(u'' + l\theta'') = F \tag{2.37}$$

and balancing the moments about the pivot point P of the payload ($\Sigma M_P = 0$) leads to

$$m(u'' + l\theta'')l\cos(\theta) + mgl\sin(\theta) = 0. \tag{2.38}$$

Using (2.37), we eliminate u in Eq. (2.38) and obtain

$$\theta'' + \tan(\theta) + h(s) = 0, \tag{2.39}$$

where prime means differentiation with respect to the dimensionless time $s \equiv \omega t$ and ω is the crane–payload frequency defined by $\omega \equiv \sqrt{(M+m)g/(Ml)}$. The external force is $h(s) \equiv F(s)/((M+m)g)$. Finally, we introduce a small damping term $(2\mu\theta')$ to take into account weak dissipation. Equation (2.39) then becomes

$$\theta'' + \tan(\theta) + 2\mu\theta' + h(s) = 0. \tag{2.40}$$

We next propose a Pyrygas-type control [191] of the form $h = k(\theta(s - \tau) - \theta)$. It has the advantage that the equilibrium point is not modified by

the feedback. Linearizing Eq.(2.39) leads to

$$\theta'' + 2\mu\theta' + \theta + k(\theta(s-\tau) - \theta) = 0. \tag{2.41}$$

The linear stability boundaries are found by introducing $\theta = \exp(i\sigma s)$ into Eq.(2.41). From the real and imaginary parts, we obtain

$$\begin{aligned} -\sigma^2 + 1 + k(\cos(\sigma\tau) - 1) &= 0, & (2.42)\\ 2\mu\sigma - k\sin(\sigma\tau) &= 0. & (2.43) \end{aligned}$$

The solution for $k = k(\tau)$ can be determined analytically. If we wish to avoid the inverse trigonometric functions, we may obtain the solution in parametric form using $x \equiv \sigma\tau/2 \geq 0$ as parameter. Eliminating k in Eqs.(2.42) and (2.43), and inserting $\sigma = 2x/\tau$, we obtain a quadratic equation for τ. It always admits a positive real root given by

$$\tau = 2\left[\mu x \tan(x) + |x|\sqrt{\mu^2\tan^2(x) + 1}\right]. \tag{2.44}$$

Having $\tau(x)$, we determine k using (2.43) with $\sigma = 2x\tau^{-1}$:

$$k = \frac{4\mu x}{\tau \sin(2x)}. \tag{2.45}$$

By continuously increasing x from zero, the successive Hopf bifurcation curves are generated by (2.44) and (2.45) (full lines in Figure 2.6). The friction coefficient μ is generally small and if $\mu = 0$, the expressions of the Hopf bifurcation lines considerably simplify. From Eqs. (2.42) and (2.43), we find the following three cases

$$\begin{aligned} k_0 &= 0 \text{ and } \sigma_0 = 1, & (2.46)\\ \tau_0 &= 2n\pi \text{ and } \sigma_0 = 1, & (2.47)\\ k_0 &= \frac{1}{2}\left[1 - (\frac{(2n+1)\pi}{\tau})^2\right] \quad \text{and} \quad \sigma_0 = \frac{(2n+1)\pi}{\tau}. & (2.48) \end{aligned}$$

where $n = 0, 1, 2, \ldots$. The horizontal line $k = 0$, the vertical line defined by (2.47) with $n = 1$, and the lines defined by (2.48) with $n = 0$ and 1 are shown by broken lines in Figure 2.6.

2.4 Traffic stability

The control of traffic congestion problems is an important problem in our society: where to install traffic lights or stop signs, how many lanes to build for a new highway, should we develop alternate forms of transportation, and so on. The desired goal is to achieve equilibrium and stability, but

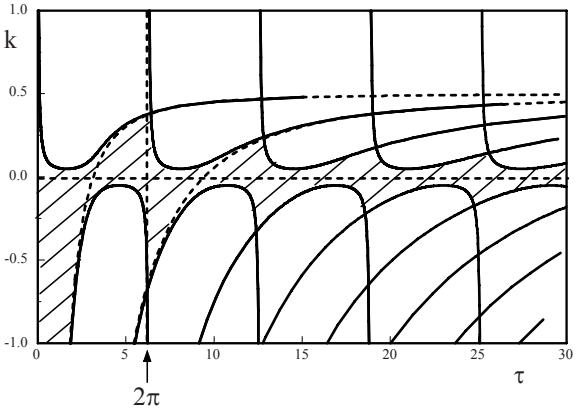

FIGURE 2.6. Successive Hopf bifurcation lines (solid) in the k versus τ parameter plane for $\mu = 0.025$. The broken lines correspond to the limiting case of no friction ($\mu = 0$) and are shown for the first four Hopf bifurcations. The crosshatched domain corresponds to a stable steady state.

this is not always attained. In heavy traffic where drivers follow each other very closely, an acceleration or deceleration of one vehicle may be a small disturbance that will be preserved or amplified in the system over time, suggesting that there can be sensitive dependence on initial conditions. This is a potential problem for traffic management, and can even result in accidents.

2.4.1 Car-following models

The starting point of a mathematical description of traffic flow problems is an equation describing the conservation of cars (cars are not created or destroyed). In one space dimension, this equation is a partial differential equation given by [83, 238, 26]

$$\rho_t + q_x = 0, \tag{2.49}$$

where $\rho(x,t)$ is the density of cars and $q(x,t)$ represents the traffic flow (in physics: the "flux" of ρ across a boundary). However, for traffic problems where u is the average velocity of cars, $q = \rho u$. We make the simplified assumption that u depends only on the density of cars; that is, $u = u(\rho)$. This function can be determined experimentally (e.g., by counting the number of cars passing per hour). It may also be determined by using simple models. The motion of a line of vehicles on a crowded road link without overtaking (a rash assumption) is described by a car-following model [33]. This model is based on the assumption that a driver responds to the motion of the vehicle immediately in front. In the simplest model, the acceleration on the

following car is assumed to be proportional to the difference between its speed and that of the car in front:

$$\frac{d^2x_n}{dt^2} = -\lambda(\frac{dx_n}{dt} - \frac{dx_{n-1}}{dt}). \tag{2.50}$$

If the car following is going faster than the preceding one, then the car following will slow down (and thus $\lambda > 0$). The larger the relative velocity, the more the car behind accelerates or decelerates. λ measures the sensitivity of the two-car interaction. However, Eq. (2.50) suggests that acceleration or deceleration occurs instantaneously. Instead, let us allow some time before the driver reacts to changes in the relative velocity. The process is modeled by specifying the acceleration at a slightly later time

$$\frac{d^2x_n(t+\tau)}{dt^2} = -\lambda(\frac{dx_n}{dt} - \frac{dx_{n-1}}{dt}), \tag{2.51}$$

where τ is the reaction time. Mathematically, this equation is a DDE. Integrating Eq. (2.51) once yields

$$\frac{dx_n(t+\tau)}{dt} = -\lambda(x_n - x_{n-1}) + d_n, \tag{2.52}$$

an equation relating the velocity of cars at a later time to the distance between cars. Imagine a steady-state situation in which all cars are equidistant apart, and hence moving at the same velocity. Thus

$$\frac{dx_n(t+\tau)}{dt} = \frac{dx_n(t)}{dt}, \tag{2.53}$$

and hence letting $d_n = d$

$$\frac{dx_n(t)}{dt} = -\lambda(x_n - x_{n-1}) + d. \tag{2.54}$$

Because

$$x_{n-1} - x_n = \frac{1}{\rho} \tag{2.55}$$

is a reasonable definition of traffic density, this model yields a velocity–density relationship

$$u = \frac{\lambda}{\rho} + d. \tag{2.56}$$

We choose the one arbitrary constant d such that at maximum density (bumper-to-bumper traffic) $u = 0$. In other words

$$0 = \frac{\lambda}{\rho_{\max}} + d. \tag{2.57}$$

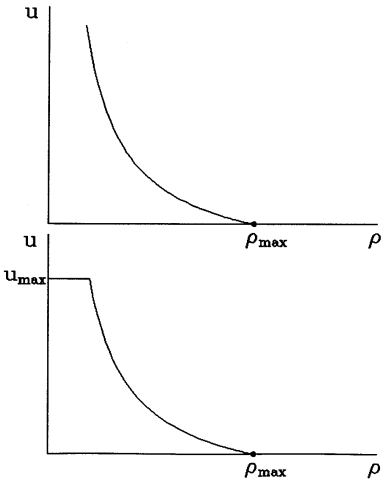

FIGURE 2.7. The speed u as a function of the density ρ. The top figure shows the hyperbolic function as predicted by the car-following model. In practice, the maximum permitted speed $u = u_{\max}$ is introduced (see bottom figure).

In this way the following velocity–density relationship is derived,

$$u = \lambda \left(\frac{1}{\rho} - \frac{1}{\rho_{\max}} \right). \tag{2.58}$$

See Figure 2.7. How does this compare with experimental observations of velocity–density relationships? Equation (2.58) appears reasonable for large densities, that is, near $\rho = \rho_{\max}$. However, it predicts an infinite velocity at zero density. We can eliminate this problem by noting that this model is not appropriate for small densities for the following reasons. At small densities, the change of speed of a car is not due to the car in front. Instead it is more likely that the speed limit influences a car's velocity (and acceleration) at small densities. Thus we may hypothesize that Eq. (2.58) is valid only for large densities. For small densities, u is only limited by the speed limit $u = u_{\max}$ (see Figure 2.7).

2.4.2 Local and asymptotic stability

When the lead vehicle of a line of cars changes its motion, the response of the following vehicle and the global response of all the cars in the line will not be the same. In this section we address this question by considering both the stability of two successive cars as well as the stability of a large numbers of cars.

Equation (2.51) can be solved by the method of Laplace transform [93] but the evaluation of the inverse Laplace transform may lead to a com-

plex expression with little physical insight. In this section, we address the stability of the linear car following Eq.(2.51) with respect to disturbances. Two particular types of stabilities need to be examined, *local stability* and *asymptotic stability*. Local stability is concerned with the response of the following vehicle to a fluctuation in the motion of the vehicle directly in front of it; that is, it concentrates on the localized behavior between pairs of vehicles. Asymptotic stability is concerned with the manner in which a fluctuation in the motion of any vehicle, say the lead vehicle of a platoon, is propagated through a line of vehicles.

Local stability

From Eq.(2.51), we determine the equation for the velocity $v_n = dx_n/dt$ given by

$$\frac{dv_n(t+\tau)}{dt} = -\lambda(v_n - v_{n-1}). \tag{2.59}$$

Consider the case of two cars traveling with equal speed u. Assuming that the lead vehicle keeps its velocity, the following vehicle $v_n = u + y$ satisfies

$$\frac{dy(t+\tau)}{dt} = -\lambda y, \tag{2.60}$$

or equivalently,

$$\frac{dy}{ds} = -\lambda\tau y(s-1), \tag{2.61}$$

where $s = t/\tau + 1$. Equation (2.61) was analyzed in Section 2.1. We know that y does not exhibit any oscillations if

$$\lambda\tau \leq e^{-1} \simeq 0.37 \tag{2.62}$$

and that y is oscillatory with exponential damping if

$$e^{-1} < \lambda\tau < \pi/2 \simeq 1.57. \tag{2.63}$$

In order for the following vehicle not to overcompensate for a fluctuation, it is necessary that condition (2.62) be verified. The criterion of local stability is often referred to this condition although the steady state is unstable only if $\lambda\tau > \pi/2$.

Asymptotic stability

Now assume that the lead driver's velocity varies periodically as

$$v_0 = 1 + \frac{1}{2}\left(\exp(i\omega t) + c.c\right). \tag{2.64}$$

Also assume that the nth driver's velocity varies periodically

$$v_n = 1 + \frac{1}{2}\left(f_n \exp(i\omega t) + c.c\right), \tag{2.65}$$

where f_n measures the amplification or decay that occurs. Starting with $f_0 = 1$, we determine f_1 as a function of f_0,then f_2 as a function of f_1, and so on. Iterating n times, the solution is given by

$$f_n = \frac{1}{\left[1 + \frac{i\omega}{\lambda}\exp(i\omega\tau)\right]} f_{n-1} = \frac{1}{\left[1 + \frac{i\omega}{\lambda}\exp(i\omega\tau)\right]^n} f_0. \tag{2.66}$$

Thus, the amplitude $|f_n|^2$ is computed as

$$\begin{aligned} |f_n|^2 &= \frac{1}{\left(1 + \frac{i\omega}{\lambda}\exp(i\omega\tau)\right)^n} \frac{1}{\left(1 - \frac{i\omega}{\lambda}\exp(-i\omega\tau)\right)^n} |f_0|^2 \\ &= \left[\frac{1}{\left(1 + \frac{\omega^2}{\lambda^2} - \frac{2\omega}{\lambda}\sin(\omega\tau)\right)}\right]^n. \end{aligned} \tag{2.67}$$

We next wish that $|f_n|^2 \to 0$ which means that

$$\frac{\omega^2}{\lambda^2} - \frac{2\omega}{\lambda}\sin(\omega\tau) > 0 \quad \text{or} \quad \frac{\omega}{\lambda} - 2\sin(\omega\tau) > 0 \quad \text{or} \quad \frac{\sin(\omega\tau)}{\omega} < \frac{1}{2\lambda}. \tag{2.68}$$

The inequality holds for all ω if [3]

$$\lambda\tau < \frac{1}{2}. \tag{2.69}$$

We conclude that if the product of the sensitivity and the time lag is greater than 0.5, it is possible for following cars to drive more erratically than the leader. In this case, we say that the model predicts instability if $\lambda\tau > \frac{1}{2}$. Note that the criterion for local stability (namely that no local oscillations occur if $\lambda\tau < e^{-1}$) also insures asymptotic stability.

2.5 Bistability

Recent experiments on polarization switching in lasers subject to optical feedback [203] have motivated a simple analytical study of a first-order DDE. The laser (here a vertical-cavity surface-emitting laser) is subject to optical feedback from a distant mirror (see Chapter 7). As a result, the light reinjected into the laser corresponds to the laser output at time $t-\tau$ where $\tau = 2L/c$. $L = 20.2$ cm being the distance laser-mirror and $c = 3\times10^8$ m/s the speed of light, we determine $\tau = 1.3$ ns. Compared to the time-scale of the laser (i.e., the photon lifetime $\tau_p \sim 1$ ps), this delay is large and we may reasonably expect some impact on the laser response. The experiments

[3] We investigate the function $\lambda = \omega/2\sin(\omega\tau)$ and note that the limit ω small leads to the stability limit.

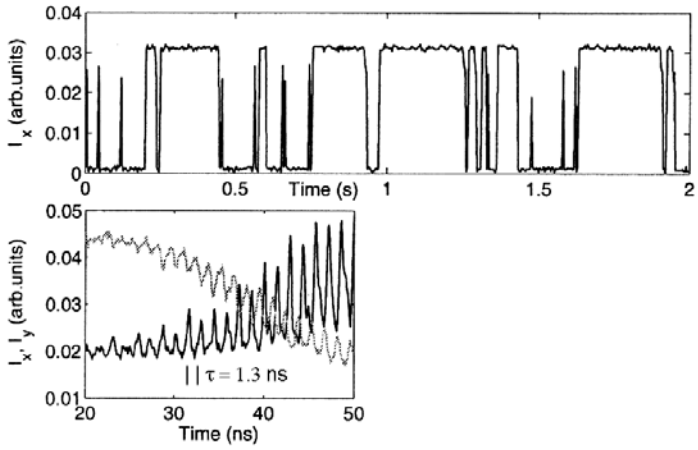

FIGURE 2.8. Top: Polarization mode-hopping. Bottom: Blow-up of the fast oscillatory jump transition between modes. The frequency $f \sim 450$ MHz is close to the inverse of the delay τ (from Sciamanna et al [203]).

indicate that the laser exhibits polarization mode hopping due to noise (i.e., spontaneous emission noise) with fast oscillatory jump transitions with a period close to τ. See Figure 2.8. These transient oscillations are not specific to the laser but have been found by numerically investigating the following first-order DDE,

$$x' = x - x^3 + cx(t-\tau) + \sqrt{2D}\xi(t) \tag{2.70}$$

where $\xi(t)$ is a Gaussian white noise of zero mean and unitary variance and D is the noise level. Equation (2.70) has been analyzed by Tsimring and Pikovsky [224] and Masoller [153] in the general context of a bistable system subject to noise. Their studies motivated further experimental work using a laser subject to a time-delayed optoelectronic feedback [101].

In this section, we illustrate the technique of linearization by examining the stability of the steady states of Eq. (2.70) with $D = 0$. It admits the following steady state-solutions

$$x = 0, \tag{2.71}$$

$$x = x_\pm \equiv \pm\sqrt{1+c}\ (c \geq -1). \tag{2.72}$$

From (2.72), we note that two non-zero steady states are branching from the zero solution at $c = -1$. Introducing the deviation $u = x - x_s$ where x_s is either (2.71) or (2.72), and assuming u small, we obtain a linear DDE. Looking then for exponential solutions leads to the following characteristic equation for the growth rate σ,

$$\sigma = 1 - 3x_s^2 + c\exp(-\sigma\tau). \tag{2.73}$$

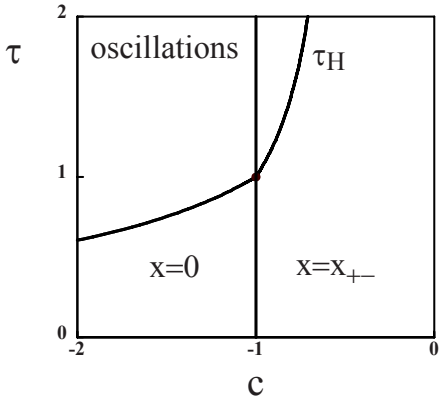

FIGURE 2.9. Stability diagram. The vertical line at $c = -1$ marks a steady bifurcation point from the zero to the non–zero steady state. The left curve connecting $(c, \tau) = (-1, 1)$ corresponds to a Hopf bifurcation point from the zero intensity steady state. The right curve starting at $(c, \tau) = (-1, 1)$ represents a Hopf bifurcation from the non–zero steady state. The critical point $(c, \tau) = (-1, 1)$ is a degenerate Hopf bifurcation point characterized by a double zero eigenvalue.

As for Eq. (2.4), we examine this equation by first considering the case σ real and then the case σ complex ($\sigma = \sigma_r + i\sigma_i$). In the first case, we determine an implicit solution for $c = c(\sigma)$ which can be analyzed. In the second case, we formulate the parametric solution $\sigma_r = \sigma_r(\sigma_i\tau)$ and $c = c(\sigma_i\tau)$ which may or may not be expressed in terms of analytical functions.

If $c < -1$, $x_s = 0$ is the only steady state. It may change stability at a Hopf bifurcation provided τ is sufficiently large. Inserting $\sigma = i\sigma_i$ into (2.73) with $x_s = 0$, we obtain

$$1 - c\cos(\sigma_i\tau) = 0, \tag{2.74}$$

$$\sigma_i + c\sin(\sigma_i\tau) = 0. \tag{2.75}$$

Equivalently, we may formulate the parametric solution

$$c = \frac{1}{\cos(s)} \quad \text{and} \quad \tau = -\frac{s}{\tan(s)}, \tag{2.76}$$

where $s = \sigma_i\tau$. If $c > -1$, $x_s = 0$ always admits a real positive σ and is therefore unstable.

For the non–zero intensity steady-states $x_s = x_\pm$, a Hopf bifurcation is possible. Inserting $\sigma = i\sigma_i$ into (2.73), we now obtain

$$-2 + c(-3 + \cos(\sigma_i\tau)) = 0, \tag{2.77}$$

$$\sigma_i + c\sin(\sigma_i\tau) = 0 \tag{2.78}$$

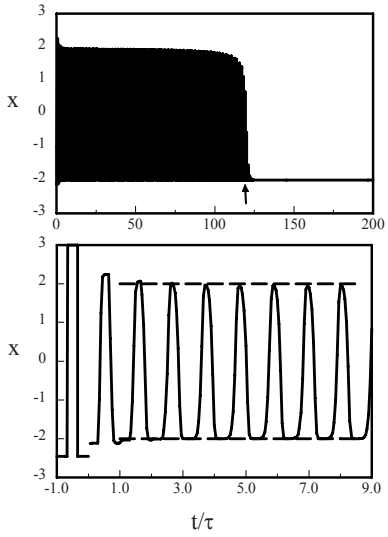

FIGURE 2.10. Top: slowly varying oscillations followed by a sudden jump to the steady-state $x = -2$. Bottom: short time solution showing the initial conditions: $x = -2.45$ ($-\tau < t < -2\tau/3$ and $-\tau/3 < t < 0$) and $x = 3$ ($-2\tau/3 < t < -\tau/3$). The values of the parameters are $c = 3$ and $\tau = 5$.

from the real and imaginary parts. These conditions can be rewritten as

$$c = -\frac{2}{3 - \cos(s)} \quad \text{and} \quad \tau = \frac{s(3 - \cos(s))}{2\sin(s)}, \tag{2.79}$$

where $s = \sigma_i \tau$. Using (2.76) and (2.79), we may represent the Hopf bifurcation line in the (c, τ) stability diagram. See Figure 2.9. There are other Hopf bifurcation lines (not shown) that appear at higher values of c or τ.

The critical point $(c, \tau) = (-1, 1)$ is a degenerate Hopf bifurcation point because it corresponds to a double zero eigenvalue of the characteristic equation. The possible solutions near this point have been analyzed in detail by Redmond et al. [196] who derived a slow time second order differential equation for the small amplitude solutions. They showed that stable time-periodic solutions may coexist with stable steady states.

2.6 Metastability

The evolution to a long time steady-state solution can be oscillatory and very slow. The numerical solution of Eq.(2.70) is shown in Figure 2.10 starting from a square wave initial profile. Figure 2.10 shows sustained oscillations with a period close to the delay that disappear on the long

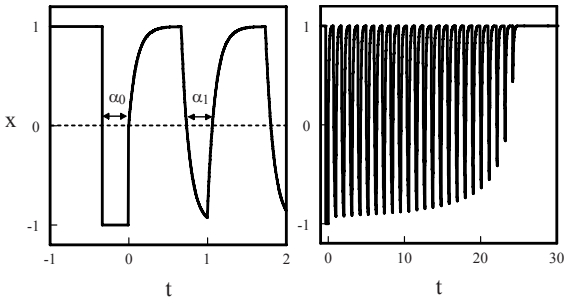

FIGURE 2.11. Right: The oscillations are slowly changing until they suddenly dissapear and are replaced by the stable steady state $x = 1$. Left: Initial oscillations showning the first two intervals between successive zeros. $\varepsilon = 0.1$ and the initial function is $x = 1$ $(0 \le t < 2/3)$, $x = -1$ $(2/3 \le t < 0)$, and $x(0) = 0$.

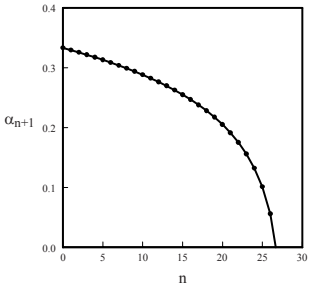

FIGURE 2.12. Progressive decrease of α_n defined as the time interval between two successive zeros of the solution. $\alpha_0 = 1/3$ and $\varepsilon = 0.1$.

time-scale. By tuning parameters, it is possible to observe the oscillations for longer periods. The phenomenon has been called *metastability*.

This phenomenon can be analyzed in detail using the following DDE,

$$\varepsilon x' = -x + f(x(t-1)), \tag{2.80}$$

where $\varepsilon = \tau^{-1}$, $f(x) = -1$ if $x < 0$, $f(x) = 1$ if $x > 0$, and $f(0) = 0$ [3]. The numerical solution is shown in Figure 2.11. By constructing the solution in successive time intervals, it is possible to formulate a map for the interval α_n between two successive zeros [81]. It is given by

$$\alpha_{n+1} = \alpha_n + \varepsilon \ln \left[\frac{2 - 2\exp(-\varepsilon^{-1}\alpha_n) + \exp(-\varepsilon^{-1})}{2 - \exp(-\varepsilon^{-1}(1-\alpha_n))} \right] \tag{2.81}$$

which for small ε and $\alpha_0 < 0.5$ simplifies as

$$\alpha_{n+1} - \alpha_n \simeq \varepsilon \exp(-\varepsilon^{-1}\alpha_n) \tag{2.82}$$

The map (2.81) and its approximation (2.82) are mathematically valid until $\alpha_n = O(\varepsilon)$. The different iterations of Eq. (2.82) are shown in Figure 2.12. The expression (2.82) clearly indicates that the rate of change is $\varepsilon \exp(-\varepsilon^{-1})$ small. As noted in [81], this small rate of change results from the fact that $f(x(t-1)) = \pm 1$ for $x \gtrless 0$. If $f(x(t-1)) = a < 0$ and $b > 0$ for $x \gtrless 0$, and if $|a| \neq b$, the rate of change is $O(\varepsilon)$. The behavior of metastable patterns is further analyzed by Nizette [176] who formulated a Ginzburg–Landau equation from a general class of DDEs.

http://www.springer.com/978-0-387-74371-4

Applied Delay Differential Equations
Erneux, Th.
2009, XII, 204 p., Softcover
ISBN: 978-0-387-74371-4